AN EXAMINATION OF THREE COMMON ASSUMPTIONS USED TO SIMULATE RECOMBINATION IN HEAVILY DOPED SILICON

Keith R. McIntosh,[1] Pietro P. Altermatt,[2] Tom J. Ratcliff,[3] Kean Chern Fong,[3]
Lachlan E. Black,[3] Simeon C. Baker-Finch,[1,3] and Malcolm D. Abbott[1]

[1] PV Lighthouse, Coledale, NSW 2515, AUSTRALIA. krmcintosh@pvlighthouse.com.au.
[2] Leibniz University of Hannover, Inst. of Solid-State Physics, Dep. Solar Energy, Appelstrasse 2, 30167, GERMANY
[3] Centre for Sustainable Energy Systems, Australian National University, Canberra, ACT 0200, AUSTRALIA

ABSTRACT: A well-designed silicon solar cell entails a complicated optimisation of its heavily doped surfaces. There exist many analytical and numerical models to assist this optimisation, and each involves a foray of assumptions. In this paper, we examine three of the common assumptions: (i) quasi-neutrality, (ii) the use of effective recombination parameters as a boundary condition at the surface, and (iii) the use of Boltzman rather than the more complicated but more precise Fermi–Dirac statistics. We examine their validity and the computational benefits of their inclusion. We find that (i) the quasi-neutrality assumption is valid over a wide range of conditions, enabling a fast and relatively simple simulation of emitter recombination, (ii) the effective surface recombination velocity depends on doping under most conditions and can give the misleading impression that the density of interface defects depend strongly on surface concentration, and (iii) at carrier concentrations where Boltzmann statistics are invalid (above 10^{19} cm^{-3}, and especially above 10^{20} cm^{-3}), it is more difficult to mitigate the error by employing an effective model that combines degeneracy with band-gap narrowing, than to include the more general Fermi–Dirac statistics themselves.
Keywords: Recombination, Simulation, Software

1 INTRODUCTION

All silicon solar cells contain heavily doped surfaces to ensure low contact resistance, low surface recombination and low lateral resistance. They are called emitters, diffusions, back-surface fields, front-surface fields and floating junctions. As the doping increases, contact resistance and lateral resistance decrease (which is good), free carrier absorption increases (bad), and recombination first decreases (good) and then increases (bad). Given these competing effects, it is desirable to optimise the dopant profiles at the surfaces, at least to within the constraints of low-cost manufacturing.

An optimisation of a cell's heavily doped surfaces—referred to as emitters from here on—is aided by the ability to accurately simulate their behaviour. This is more easily said than done. The dopant concentration varies over many orders of magnitude in a short distance causing significant variations in the minority carrier concentration, Auger recombination, Shockley–Read–Hall recombination, carrier mobility, free-carrier absorption, effective masses, and last but not least, the band gap. Moreover, when the emitter is heavily doped, the semiconductor becomes degenerate and the carrier concentrations must be calculated with Fermi–Dirac statistics rather than the simpler Boltzmann statistics. More complicated still, the surface of an emitter constitutes an interface with a different material, which necessarily introduces interface defects and the possibility of surface charge.

There are many analytical and numerical models for simulating emitters. In this paper, we discuss three of the assumptions that are employed in many of those models: (1) quasi-neutrality, (2) the effective recombination velocity as a boundary condition, and (3) Boltzmann statistics. We describe conditions under which they are valid and invalid.

2 SIMULATION TOOLS

We employ EDNA 2 [1, 2] to represent a model containing the quasi-neutrality assumption and PC1D [3] and Sentaurus [4] to represent models that do not.

EDNA 2 is an online computer simulation program that models recombination in a 1D emitter. It is based on the freeware Excel model released in 2010 [2]. As well as being much faster than its predecessor, EDNA 2 has additional features:

- models for incomplete ionisation of dopant atoms;
- a selection of models for carrier mobility;
- the choice of Fermi–Dirac or Boltzmann statistics that is independent of the selected band-gap narrowing model;
- the ability to sweep input parameters to generate plots such as J_{0E} vs surface concentration;
- the choice of setting S_{eff}, J_{0s}, and soon, the full set of interface properties ($D_{it}(E)$, $\sigma_p(E)$, $\sigma_n(E)$, and Q) to parameterise surface recombination; and
- the option to set a J_{0E} and determine surface parameters.

EDNA 2 runs on a cloud-based server that has high computation speeds. The principle reason, however, that the computation time is short relative to its alternatives is that EDNA 2 assumes the emitter is 'quasi neutral'. It is also specifically designed to rapidly determine an emitter's recombination parameters like J_{0E} and IQE. It does not solve a complete device but solely the emitter, which introduces error when recombination in or near the depletion region is significant.

Sentaurus is the most complete and accurate approach to modelling semiconductor devices. For simulating emitters, it has practically all of the functionality of EDNA 2 and far more besides. It does not assume quasi-neutrality, it allows 2D and 3D devices, and it simulates complete and sophisticated devices [4].

PC1D is the most commonly used program for simulating solar cells. It is limited to Boltzmann and a single model for carrier mobility, band-gap narrowing and Auger recombination. It does not assume quasi-

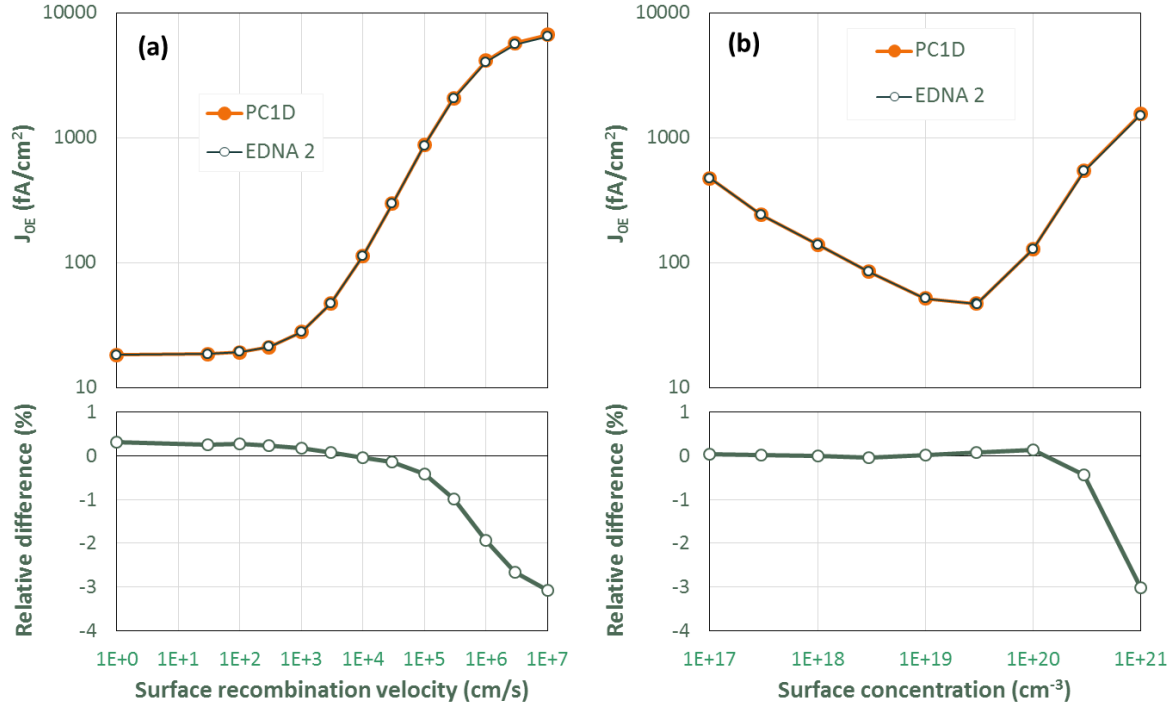

Figure 1: The upper graphs plot J_{0E} determined from PC1D and EDNA 2 as a function of **(a)** surface recombination velocity S_{eff} with surface dopant concentration $N_S = 3.05 \times 10^{19}$ cm^{-3} and **(b)** N_s with $S_{eff} = 3000$ cm/s; the lower graphs plot the relative difference in J_{0E} determined by EDNA 2 compared to the J_{0E} determined by PC1D.

neutrality, it simulates complete 1D devices, and it is fast, free and open source [3].

3 ASSUMPTION 1: QUASI-NEUTRALITY

The quasi-neutrality (QN) assumption states that the excess hole concentration Δp equals the excess electron concentration Δn. This assumption is contained in many recent solar cell programs [1, 2, 5–7] and in many analytical emitter models [e.g, 8–10]. The Shockley diode equation is also limited to the QN regions of the cell.

When the QN assumption is applied, the carrier concentrations can be determined without recourse to the electric field. That is, the three coupled differential equations that relate the electron concentration n, the hole concentration p, and the electric field (or potential ψ) can be simplified into one differential equation, making it much simpler and faster to solve.

The QN assumption is valid in regions where the electric field is small. It becomes increasingly invalid as the gradient of the excess carriers increases, and it is entirely invalid in a depletion region (where the electric field is large). The QN assumption is also invalid near the surface when surface charge is significant (i.e., when the surface is in accumulation, depletion or inversion).

In this section, we examine the applicability of the QN assumption for emitter modelling. It is conducted by comparing the results of EDNA 2 with PC1D and Sentaurus.

Figure 1 plots the results of the comparison between EDNA 2 and PC1D. This first comparison contains simple physical models, such as Boltmann statistics, constant carrier mobilities, and an exponential apparent band-gap narrowing model. Figure 2 plots the results of the comparison between EDNA 2 and Sentaurus. This second comparison contains more sophisticated models, including Fermi–Dirac statistics, Klaassen's mobility model, and Schenk's band-gap narrowing. Appendix A describes the simulation inputs in labourious detail.

The upper graphs in Figures 1 and 2 plot the J_{0E} determined from the programs as a function of (a) surface recombination velocity and (b) surface dopant concentration N_s. The figures indicates a close agreement between EDNA 2 and PC1D for the simpler comparison, and between EDNA 2 and Sentaurus for the more sophisticated comparison.

The lower graphs in Figures 1 and 2 plot the relative difference between the simulations; they show that J_{0E} determined by EDNA 2 tends to be a little less than that determined by PC1D or Sentaurus, but by no more than 4% over the tested range of inputs (except for the most heavily doped diffusion in the comparison wit Sentaurus, for which it is 6% smaller). The source of these small discrepancies was not determined.

It is concluded from this study that, over a wide variety of emitters, and with and without sophisticated semiconductor models, the QN assumption can be imposed with little loss in accuracy. The error introduced into the emitter's J_{0E} by the QN assumption is within the range +0.3% to –6%.

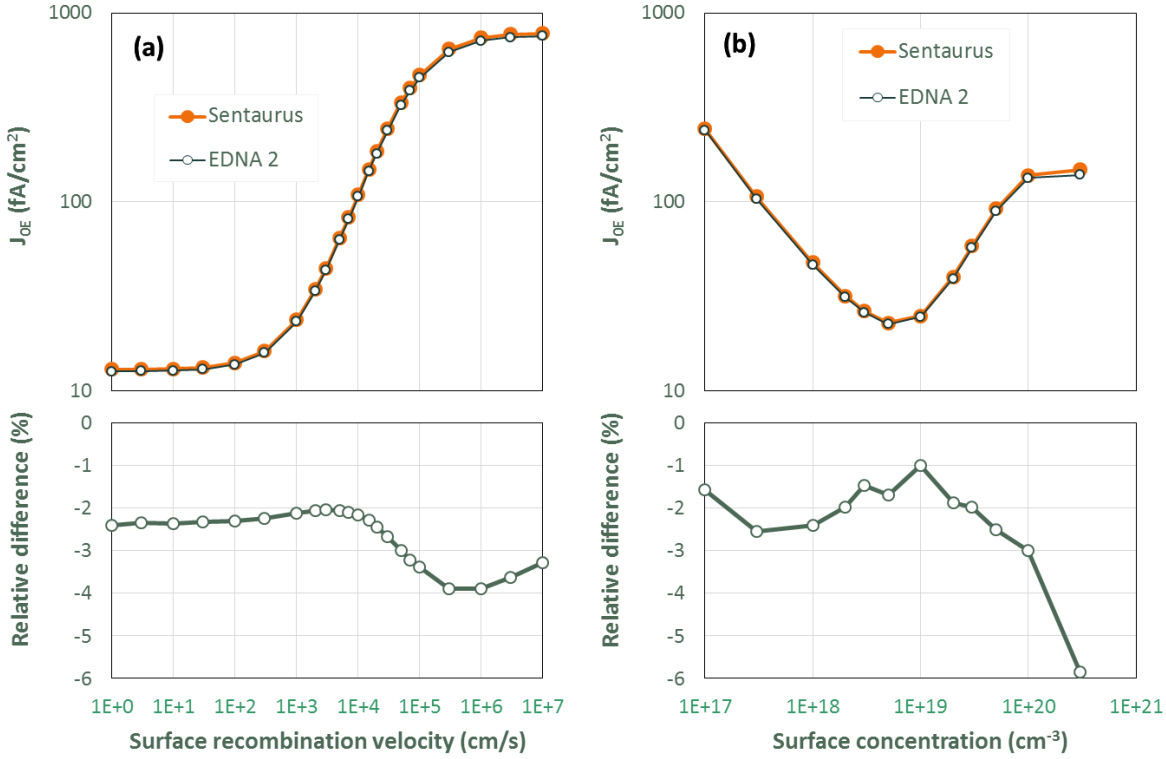

Figure 2: The upper graphs plot J_{0E} determined from Sentaurs and EDNA 2 as a function of **(a)** S_{eff} with $N_S = 1 \times 10^{19}$ cm^{-3} and **(b)** N_s with S_{eff} = 1000 cm/s; the lower graphs plot the relative difference in J_{0E} determined by EDNA 2 compared to J_{0E} determined by Sentaurus.

4 ASSUMPTION 2: THE EFFECTIVE SURFACE RECOMBINATION VELOCITY

4.1 Introduction to S_{eff}

A well-known parameter that quantifies surface passivation is the effective surface recombination velocity S_{eff}. It is employed as a boundary condition in the current versions of Quokka [5], CoBoGUI [11, 12] and EDNA [1, 2], as well as a host of analytical equations [8–10].

The merit in using S_{eff} is that it incorporates many aspects of surface recombination into a single parameter. Specifically, it combines the interface state density $D_{it}(E)$, the capture cross section of electrons $\sigma_n(E)$ and holes $\sigma_p(E)$, and the net surface charge Q whether it be in an insulator or at an insulator–semiconductor interface. The drawback in using S_{eff} is that by lumping various physical phenomena together, it is difficult to recognise the physical reasons behind its behaviour. Under some conditions, for example, the application of S_{eff} can be misleading, making it easy to use erroneous values of S_{eff} during emitter simulations.

When Q is significant, S_{eff} becomes dependent on the surface dopant concentration N_s, even when the actual SRH surface recombination velocity parameters, S_{n0} and S_{p0}, are independent of N_s [13–15]. Plots of S_{eff} against N_s invariably exhibit a strong increase of S_{eff} with N_s, and it has subsequently been construed that the surface defect density must increase with N_s when in fact there might be no such evidence. This is not to say that the defect density cannot increase with N_s, only that it might not necessarily increase with N_s. In fact, for Al_2O_3–Si interfaces, it has recently be concluded that S_{n0} and Q are relatively constant over a wide range of N_s [17].

In this section, we describe the conditions under which S_{eff} is independent of N_s. We also describe an alternative surface parameter J_{0s} that is independent of N_s when the surface charge is large [18]. (The J_{0s} is analogous to the popular emitter saturation current density J_{0E}, as described in Section 4.3). The purpose of employing these quasi-parameters is that (i) they represent a single metric for the quality of a surface passivation scheme, and (ii) they can readily measured by conventional lifetime measurements on undiffused silicon.

4.2 The dependence of S_{eff} on N_s

The effective surface recombination velocity S_{eff} is defined as

$$J_{rec} = q \cdot U_s = q \cdot S_{eff} \cdot \Delta n_d \qquad (1)$$

where J_{rec} is the current density that flows into the surface to recombine, q is the charge of an electron, U_s is the recombination rate at the surface in cm^{-2}s^{-1}, and Δn_d is the excess carrier concentration 'near' the surface. The subscript d refers to the distance from the surface at which the carrier concentrations are no longer affected by surface charge. This is illustrated in Figure 3. Usually this distance is sufficiently close to the surface s that there is negligible difference between the doping concentration at s and d. The recombination and generation rates between s and d tend to be negligible compared to U_s.

We now derive S_{eff} for an *n*-type emitter. In this case, electrons are the majority carriers and holes are the minority carriers. More detailed derivations are given in [13–18].

Due to the high dopant concentration at *d*, Equation 1 can be rewritten

$$S_{eff} = U_s / p_d \,, \qquad (2)$$

where p_d is the hole concentration at *d* and equal to Δn_d (since the excess carrier concentration is the same for electrons and holes when quasi-neutrality is valid).

Now, at *s*, the hole concentration is far smaller than the electron concentration, so Shockley–Read–Hall (SRH) recombination at the surface can be given by the simple relation,

$$U_s = S_{p0} \cdot p_s \qquad (3)$$

where S_{p0} is the hole recombination velocity, which depends solely on the surface defects, i.e. $S_{p0} = N_d v_{th} \sigma_p$. In fact, Equation 3 is valid only under the provisos that (i) the principle defect is within the quasi-Fermi levels of trapped charges; (ii) $n_s/\sigma_p >> p_s/\sigma_n$, which is valid in an *n*-type emitter except when there is a large negative charge at the surface; and (iii) the surface concentrations are not near their equilibrium values (i.e. $p_s n_s >> n_i^2$), which is valid in all conditions except in the dark with little or no applied bias. That may sound like a lot of provisos, but they are regularly justifiable for an emitter.

When *Q* is too small to affect the carrier concentrations, $p_s = p_d$, and Equations 2 and 3 combine to give,

$$S_{eff} = S_{p0}. \qquad (4)$$

This states that in this case S_{eff} depends solely on the surface defects and is independent of *Q* of N_s. This equality is regularly assumed (despite often being unjustified!).

When *Q* is sufficiently large that it alters the carrier concentrations near the surface, there is $p_s \neq p_d$. This is represented by the band-bending depicted in Figure 3. In such case, and when the quasi-Fermi levels are constant between *s* and *d*, $p_s = p_d \cdot \exp(\psi_s/V_T)$, where ψ_s is the band-bending in Volts and V_T is the thermal voltage. Hence,

$$S_{eff} = S_{p0} \cdot \frac{p_s}{p_d} = S_{p0} \cdot \exp\left(\frac{\psi_s}{V_T}\right). \qquad (5)$$

Equation 5 states that S_{eff} is less than S_{p0} when *Q* is positive (because minority carrier holes are repelled from the surface, making the bands bend upwards and ψ_s negative); and S_{eff} is greater than S_{p0} when *Q* is negative (ψ_s is positive).

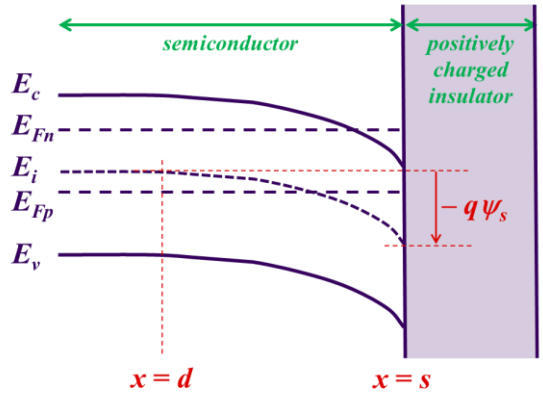

Figure 3: Band diagram at the surface of an illuminated *n*-type semiconductor coated with a positively charged insulator.

If ψ_s were dependent solely on *Q*, then S_{eff} would depend only on the surface defects and *Q*, making it a convenient and uncomplicated metric to quantify the surface passivation provided by a charged dielectric. But ψ_s also depends on N_s and Δn_d [13–21]. This means that when *Q* is significant, S_{eff} is not just related to the surface defects, but also to the doping and the excess carrier concentration. Being unaware of this dependence makes it easy to misinterpret a plot of S_{eff} against N_s and to conclude that S_{p0} increases with doping when it might not!

Figure 4 shows the conditions under which ψ_s is sufficiently small that there is no doping dependence under accumulation or inversion. This region is coloured yellow. It indicates that for typical undiffused wafers ($N_s < 10^{16}$ cm^{-3}), S_{eff} is probably never constant with doping, since it is unlikely that *Q* would ever be smaller than 3×10^9 cm^{-2}. Consequently, using S_{eff} to represent surface passivation has no merit without also stating N_s. Thus, for undiffused wafers, one cannot determine S_{eff} at some N_s and apply it at another N_s, even if S_{n0} and *Q* are independent of N_s.

Figure 4 also shows that for dopant-diffused wafers ($N_s > 10^{18}$ cm^{-3}), S_{eff} is only constant when there is small to moderate *Q*. Has *Q* ever been measured for diffused silicon? Is it possible that the apparent dependence of S_{eff} on N_s previously observed for Ph-doped SiO_2–Si

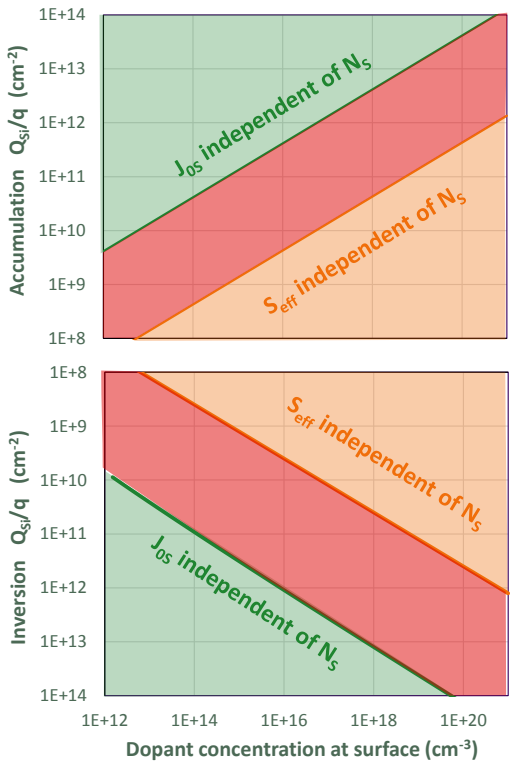

Figure 4: Contours of *Q* vs N_s at which one can assume J_{0s} and S_{eff} are independent of N_s in equilibrium. The contours represent a 10% error in the calculation of surface carrier concentration and therefore U_s, for low injection, c-Si, and 300 K; valid for either p- or n-type.

interfaces (e.g., [22–26]) is in fact due to a large Q? For some surface treatments, S_{eff} of B-doped silicon was found to vary little over N_s = 3–300 × 10^{17} cm^{-3} [27]; and in a recent study of Al_2O_3–Si, it was concluded that neither Q nor S_{p0} varied over a wide range of B-doped N_s [17].

We take this opportunity to re-evaluate previously published data for SiN_x-passivated Ph-diffused silicon [26]. In that study, S_{eff} was extracted from simulations of J_{0e} measurements. Zero surface charge Q was assumed, and the blue line in Fig. 5 was obtained [26], indicating that S_{eff} increases strongly with the phosphorus dopant density at the surface N_s. We repeated those simulations, for a constant Q of +2 and +3 × 10^{12} C/cm^2, as is typically measured at low dopant densities for SiN_x. We then plot S_{p0} (not S_{eff} because electrostatics are now considered) against N_s as the green and red lines in Fig. 5. By including this plausible level of surface charge in the calculations, we find that S_{p0} increases only slowly over the range N_s = 1 to ~7 × 10^{19} cm^{-3}. At higher N_s, S_{p0} might be overestimated because we neglect phosphorus precipitation, which often occurs at high N_s and introduces additional SRH recombination. S_{p0} is a direct measure of interface quality effects. That it appears rather insensitive to N_s might be explained by (i) the P atoms have 5 instead of 4 valence bonds, which may give an additional degree of freedom to the lattice for relaxing the twisted, stretched and dangling bonds at the interface, or (ii) dopant states may simply introduce very few defect states at the interface.

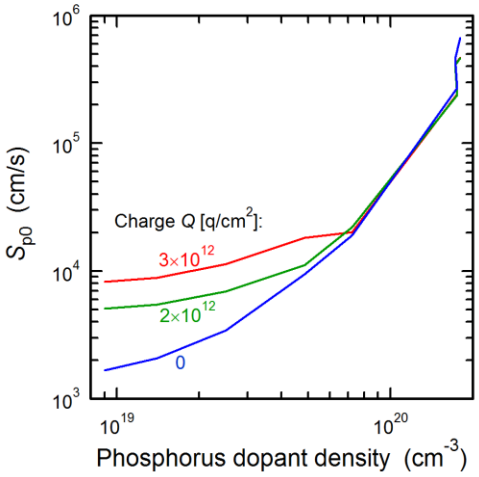

Figure 5: The surface recombination velocity parameter S_{p0} of SiN_x-passivated surfaces and its dependence on the phosphorus dopant concentration at the surface, assuming the indicated interface charge Q. S_{p0} is extracted from simulations of J_{0E} measurements as in Ref. [26].

4.3 The surface saturation current density J_{0s}

An alternative to S_{eff} is the "surface recombination current density" J_{0s}, which is introduced in Ref. [18]. Contrary to S_{eff}, it is independent of N_s when Q is large but proportional to N_s when Q is small. Thus, it is preferable to use J_{0s} when Q is large, and S_{eff} when Q is small.

The green region in Figure 4 is where J_{0s} is independent of N_s. To be more specific, the contours in Figure 4 show the points where there is a 10% error in the minority carrier concentration at the surface. Three of the four contours are governed by the ratio Q^2/N_s, where Q^2/N_s = 1.50 × 10^7 cm for the green line in accumulation, 1900 cm for the yellow line in accumulation, and 1600 cm for the yellow line in inversion. The green line in inversion does not have an explicit solution but is approximately $Q^{1.85}/N_s$ = 1.5 × 10^6 cm.

The definition of J_{0s} is in analogy to the saturation current in the Shockley diode equation. It is given by

$$J_{rec} = q \cdot U_s = J_{0s} \cdot \left[\frac{p_s n_s}{n_{is}^2} - 1\right]. \quad (6)$$

When the quasi-Fermi levels are flat between s and d, this is equivalent to

$$J_{rec} = q \cdot U_s = J_{0s} \cdot \left[\frac{p_d n_d}{n_{id}^2} - 1\right]. \quad (7)$$

and when Boltzmann statistics apply,

$$J_{rec} = J_{0s} \cdot \left[\exp\left(\frac{V}{V_T}\right) - 1\right], \quad (8)$$

where V is the separation of quasi-Fermi levels. The definition of J_{0s} is examined in more detail in Ref. [18].

When Q is sufficiently large that J_{0s} is constant with N_s (whether in accumulation or inversion), J_{0s} can be succinctly written in terms of S_{p0} and Q [13, 18]:

$$J_{0s} = q \cdot S_{p0} \frac{2kT\epsilon_{Si}}{Q^2} \cdot n_{is}^2. \quad (9)$$

4.4 Summary

We presented the conditions under which S_{eff} and J_{0s} are independent of N_s and showed how they relate to Q and S_{p0} (or S_{n0}). When neither S_{eff} nor J_{0s} can be justifiably applied, emitters cannot be accurately modelled without accounting for Q and N_s, and solutions can be found in the manner of Refs. [28, 29]. Preferably, this is performed with inputs for the energy dependent density of states of each donor and acceptor defect, their associated capture cross sections, and insulator charge.

We also note that S_{p0} and Q for Al_2O_3–Si interface have recently been found to be constant over a wide range of N_s [17] for several different deposition and annealing conditions. In passivation schemes where this is the case, emitter modelling far simpler than is currently appreciated, since one can then measure S_{p0} and Q on an undiffused sample and apply those values at any other N_s. Over certain ranges of N_s (see Figure 4), one can also combine S_{p0} and Q into a single parameter (either S_{eff} from Equation 4 or J_{0s} from Equation 9), making emitter simulation simpler and faster.

5 ASSUMPTION 3: BOLTZMANN STATISTICS.

In non-degenerate semiconductors, the number of free carriers is small relative to the number of states that those carriers can occupy. The conentration of electrons and holes can therefore be described by ideal-gas theory. When this assumption is valid, Boltzmann (B) statistics are applicable and the concentration of free electrons depends exponentially on the Fermi energy,

$$n = N_C \exp\left(\frac{E_{fn} - E_C}{kT}\right). \quad (10)$$

An equivalent equation exists for holes.

B statistics do not accurately determine the majority carrier concentration when carrier–carrier interactions are

significant. In c-Si at 300 K, this occurs when the doping exceeds 10^{19} cm^{-3} [26]. In such case, the more general Fermi–Dirac (FD) statistics are required, by which

$$n = N_C \, \mathrm{F}_{1/2}\left(\frac{E_{fn}-E_c}{kT}\right). \qquad (11)$$

Figure 6 shows how the application of (10) rather than (11) introduces error at high phosphorus dopant concentrations. In Figure 6(a), the equilibrium hole concentration p_0 (i.e., the minority carrier concentration) is plotted as a function of the ionised dopant concentration N_D when one applies B (green) and FD (orange) statistics. The dashed lines show p_0 when band-gap narrowing (BGN) is omitted and the solid lines show p_0 when BGN is included using Schenk's model for BGN [30, 2]. The figure shows a marked deviation between B and FD statistics at $N_D > 10^{19}$ cm^{-3}.

Figure 6(b) plots the relative error in p_0 when B statistics are used instead of FD. (The error is the same with or without BGN). The figure indicates that the relative error in p_0 is 10% at 10^{19} cm^{-3} and over 100% at 10^{20} cm^{-3}. Note that p_0 is overestimated by B statistics and, consequently, the calculated recombination is also overestimated, especially at $N_D > 10^{20}$ cm^{-3} where Pauli-blocking becomes significant. This ultimately leads to an overestimation of J_{0E} when modelling heavily doped emitters with (10). The amount to which J_{0E} is overestimated has a complicated dependence on the dopant profile and surface recombination.

In addition to degeneracy, BGN also causes a deviation in p_0 at high doping [26]. As evident in Figure 5, the deviation due to BGN occurs at a lower N_D (~ 10^{17} cm^{-3}), and the effect on p_0 is the opposite to that caused by degeneracy.

The opposing trends introduced by degeneracy and BGN make $p_0(N_D)$ reasonably 'exponential' until $N_D > 10^{20}$ cm^{-3} (see the solid orange line in Figure 5). This has been observed and exploited in a number of studies (e.g., [22–25, 27, 38, 39]). They find that the influence of degeneracy and BGN can be adequately combined into a simple exponential for $N_D < 10^{20}$ cm^{-3}, and thus the equations for B statistics can still be used by introducing 'apparent BGN' that combines degeneracy and BGN.

A recent example from Yan and Cuevas is plotted in Fig. 6(a) as the dotted black line [36]. Its equation is

$$n = N_C \exp\left(\frac{E_{fn}-E_c^0+E_{degBGN}}{kT}\right), \qquad (12)$$

where $E_{degBGN} = 13.0 \times 10^{-3} \cdot [\ln(N_D/10^{17})]$ in meV for $N_D > 10^{17}$ cm^{-3} and zero otherwise, $E_c{}^0$ is the equilibrium conduction band energy. A similar equation is employed in PC1D [3].

Although there are various inconsistencies by applying this approach [31, 32], the inclusion of an exponential apparent BGN describes $p_0(N_D)$ very well for $N_D < 10^{20}$ cm^{-3}. At higher N_D, Pauli-blocking becomes strong, and the apparent BGN would need to decrease strongly to account for the increasing influence of degeneracy. To our knowledge, there is no apparent model that describes this "turning point", and thus, industrial phosphorus-diffused emitters, which typically have $N_D > 10^{20}$ cm^{-3}, cannot yet be accurately modelled by apparent BGN models.

FD statistics are often avoided because $F_{1/2}$ cannot be rigorously expressed analytically. But there exist many explicit approximations [33–35] to the FD integral that significantly reduce computation time while introducing little error. Having evaluated various options, we implemented the algorithm described in [34] into EDNA 2. Compared to a fine-resolution numerical solution of the integral, the approximation gives a 100-fold reduction in computation time at a maximum cost of 0.002% relative error for Fermi levels within 100·kT of the band edges. We also rely on an analytical approximation to facilitate rapid evaluation of the inverse FD function [35]; this algorithm introduces less than 0.003% relative error in the carrier concentrations within the aforementioned range of Fermi levels (±100·kT from the band edge).

Thus, with fast and accurate application of FD statistics, we conclude that for heavily doped silicon it is preferable to account for degeneracy correctly, and to apply a separate model for BGN. Yan and Cuevas give such an option determined from experimental data for $N_D < 10^{20}$ cm^{-3}:

$$n = N_C \, \mathrm{F}_{1/2}\left(\frac{E_{fn}-(E_c^0-\Delta E_c)}{kT}\right), \qquad (13)$$

where $\Delta E_c = 4.2 \times 10^{-5} \cdot [\ln(N_D/10^{14})]^3$ for $N_D < 10^{20}$ cm^{-3} [36].

We emphasise, however, that the simulation of very heavily doped emitters is problematic irrespective of whether FD statistics are implemented. The main reason is that phosphorus precipitates readily in silicon and causes, in many cases, more SRH recombination than there is Auger recombination [37]. The precipitates are stable under usual processing conditions, e.g., during drive-in, and therefore may affect a whole series of experiments consistently (potentially in experimental studies designed to determine BGN). This consistency may give the impression that the SRH recombination can

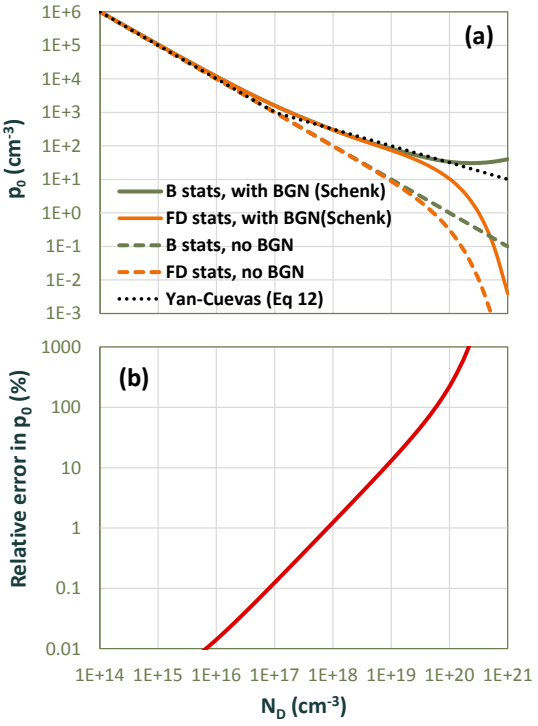

Figure 6: **(a)** Equilibrium minority carrier concentration p_0 as a function of the ionised phosphorus concentration N_D, and **(b)** relative error in p_0 by applying B instead of FD stats.

be included as an apparent BGN expression. However, such apparent BGN models only work for certain amounts of precipitation and do not have general applicability. Moreover, inactive phosphorus usually exists in various forms to various relative amounts, from interstitial phosphorus atoms, inactive phosphorus clusters, fine silicon phosphide (SiP) precipitates, to rod-like precipitate structures. Hence, we do not expect that such an apparent BGN expression can ever be universally applicable.

Apart from precipitates, there are additional uncertainties in simulating very heavily doped emitters: (i) the minority carrier mobility is not very well known in heavily doped silicon; (ii) Auger coefficients are not well established for high dopant concentrations; and (iii) the effective electron mass starts to increase above $N_D > 10^{20}$ cm^{-3}, which is neglected in Schenk's BGN model.

Because $POCl_3$ furnaces are a very cheap means of forming an emitter, it can be expected that highly doped emitters will continue to be used in the commercial production of silicon solar cells. Thus, the development of accurate simulation models for $N_s > 10^{20}$ cm^{-3} is not just enjoyable, it has industrial relevance as well.

6 REFERENCES

[1] EDNA 2 available at www.pvlighthouse.com.au.

[2] K.R. McIntosh and P.P. Altermatt, "A freeware 1D emitter model for silicon solar cells," *Proc. 35th IEEE PVSC*, Honolulu, pp. 2188–2193, 2010.

[3] P. A. Basore and D. A. Clugston, *Proc. 25th IEEE PVSC*, Washington DC, pp. 211–214, 1996.

[4] SENTAURUS, Synopsys Inc. Mountain View, CA, www.synopsys.com/products/tcad/tcad.html.

[5] A. Fell, "A free and fast 3D/2D solar cell simulator featuring conductive boundary and quasi-neutrality approximations," *IEEE Transactions on Electron Devices* **60**, pp. 733–738, 2013.

[6] P.A. Basore and K. Cabanas-Holmen, "PC2D: A circular-reference spreadsheet solar cell device simulator," *IEEE Journal of Photovoltaics* **1**, pp. 72–77, 2011.

[7] A. Cuevas and R.A. Sinton, "Detailed modelling of silicon solar cells," *Proc. 23rd EU PVSEC*, Spain, pp. 315–319. 2008.

[8] J.A. del Alamo, and R.M. Swanson, *IEEE Transactions on Electron Devices* **31**, 1878–1888 (1984);

[9] A. Cuevas and M. A. Balbuena, *IEEE Transactions on Electron Devices* **36**, 553–560 (1989);

[10] A. Cuevas, R. Merchán, and J. C. Ramos, *IEEE Tranactions on. Electron Devices* **40**, 1181–1183 (1993).

[11] R. Brendel, "Modeling solar cells with the dopant-diffused layers treated as conductive boundaries," *Progress in Photovoltaics* **20** (1), pp. 31–43, 2012;

[12] S. Eidelloth, U. Eitner, S. Steingrube and R. Brendel, "Open source graphical user interface in MATLAB for two-dimensional simulations solving the fully coupled semiconductor equations using COMSOL," *Proc. 25th EU PVSEC*, Valencia, pp. 2477–2485, 2010.

[13] B. Kuhlmann, *Charakterisierung und mehrdimensionale Simulation von MIS-Inversionsschichtsolarzellen*. PhD Thesis, Univ. Hannover, Germany, 1998.

[14] J. Brody and A. Rohatgi, "Analytical approximation of effective surface recombination velocity of dielectric-passivated p-type silicon," *Solid-State Electronics* **45**, pp. 1549 –1557, 2001.

[15] S. Steingrube, P.P. Altermatt, D.S. Steingrube J. Schmidt, R. Brendel, "Interpretation of recombination at c-Si/SiN_x interfaces by surface damage," *Journal of Applied Physics* **108**, 013506, 2010.

[17] L.E. Black, T. Allen, K.R. McIntosh and A. Cuevas, "Surface passivation of crystalline silicon by Al_2O_3: dependence on surface boron concentration," In preparation, 2013.

[18] K.R. McIntosh and L.E. Black, "On the analytical equations for field-effect passivation," In preparation, 2013.

[19] R.H. Kingston and S.F. Neustadter, *J. Appl. Phys*. **26**, p. 718, 1955.

[20] C.E. Young, *J. Appl. Phys*. **32**, p. 329,1961.

[21] A.S. Grove and D.J. Fitzgerald, *Solid-State Electron*. **9**, p. 783, 1966.

[22] A. Cuevas, P.A. Basore, G. Giroult–Matlakowski and C Dubois, "Surface recombination velocity of highly doped n-type silicon," *Journal of Applied Physics* **80**, pp. 3370–3375, 1996.

[23] S. W. Glunz, S. Sterk, R. Steeman, W. Warta, J. Knobloch, and W. Wettling, *13th EU PVSEC*, Nice, pp. 409–412,1995.

[24] M.J. Kerr, J. Schmidt, A. Cuevas and J.H. Bultman, "Surface recombination velocity of phosphorus-diffused silicon solar cell emitters passivated with plasma enhanced chemical vapor deposited silicon nitride and thermal silicon oxide," *Journal of Applied Physics* **89**, pp. 3821–3826, 2001.

[25] R.R. King, R.A. Sinton and R.M. Swanson, "Studies of diffused phosphorus emitters: Saturation current, surface recombination velocity, and quantum efficiency," *IEEE Transactions on Electron Devices* **37**, pp. 365–371, 1990.

[26] P. P. Altermatt, J. Schumacher, A. Cuevas, M.J. Kerr, S.W. Glunz, R.R. King, G. Heiser and A. Schenk, "Numerical modeling of highly doped Si:P emitters based on Fermi-Dirac statistics and self-consistent material parameters," *J. Appl. Phys*. **92**, 3187–3197 (2002).

[27] R.R. King, R.A. Sinton, and R.M. Swanson, "Studies of diffused boron emitters: Saturation current, band-gap narrowing and surface recombination velocity," *IEEE Transactions on Electron Devices* **38**, pp. 1399–1409, 1991.

[28] R.B.M. Girisch, R.P. Mertens, and R. F. De Keersmaecker, "Determination of Si-$Si0_2$ interface recombination parameters using a gate-controlled point-junction diode under illumination," *IEEE Trans. Electron Devices* **35**, 203–222 (1988).

[29] A.G. Aberle, S. Glunz and W. Warta, "Impact of illumination level and oxide parameters on Shockley–Read–Hall recombination at the Si–SiO_2 interface," *Journal of Applied Physics* **71** (9), pp. 4422–4431, 1992.

[30] A. Schenk, "Finite-temperature full random-phase approximation model of band gap narrowing for silicon device simulation," *Journal of Applied Physcis* **84**, pp. 3684–3695, 1998.

[31] H. Kroemer, "Quasi-electric and quasi-magnetic fields in nonuniform semiconductors", RCA Rev. 28, 332 (1957).

[32] M. S. Lundstrom, R. J. Schwartz, and J. L. Gray, "Transport equations for the analysis of heavily doped semiconductor devices", Solid-State Electron. 24, 195 (1981).
[33] J. S. Blakemore, "Approximations for Fermi-Dirac integrals, especially the function $F_{1/2}(\eta)$ used to describe electron density in a semiconductor", Solid-State Electronics 25, 1067-1076 (1982).
[34] Van Halen, P and Pulfrey DL. "Accurate short series approximations to Fermi–Dirac integrals of order −1/2, 1/2, 1, 3/2, 2, 5/2, 3, and 7/2," Journal of Applied Physics, 57(12), 1985; pp. 5271-5274.
[35] Antia, HM. "Rational function approximations for Fermi-Dirac Integrals," The Astrophysical Journal Supplement Series, 84, 1993; pp. 101-108.
[36] Di. Yan and A. Cuevas, "Empirical determination of the energy band gap narrowing in highly doped n+ silicon," *Journal of Applied Physics* **114**, 044508, 2013.
[37] P. Ostoja, S. Guerri, P. Negrini, S. Solmi, "The effects of phosphorus precipitation on the open-circuit voltage in n+/p silicon solar cells", Solar Cells 11, 1-12 (1984)
[38] J. del Alamo, S. Swirhun, and R. M. Swanson, "Simulataneous measurement of hole lifetime, hole mobility and band-gap narrowing in heavily doped n-type silicon, *IEEE PVSC*, 1985.
[39] J. Del Alamo, S. Swirhun and R.M. Swanson, "Measure and modelling minority carrier transport in heavily doped silicon," *Solid-State Electronics* **28**, pp. 47–54, 1985.

APPENDIX A: INPUTS IN SIMULATIONS

A.1 Comparison of EDNA 2 to PC1D

The temperature was 300 K. The bulk was *p*-type with $N_A = 1.335 \times 10^{15}$ cm^{-3}. The diffusion was *p*-type with an ERFC profile defined by a depth factor of 0.5 μm and a variable surface concentration. The intrinsic carrier concentration was 10^{10} cm^{-3} (where in EDNA 2 this was attained with the Passler model for the intrinsic band gap, Sentaurus Formula 2 for the density of states, and a band gap multiplier of 1.00385). PC1D defaults were used for band gap narrowing (i.e., del Alamo model with an onset of 1.4×10^{10} cm^{-3} and a slope of 0.014 eV), Auger recombination ($C_{n\,LLI} = 2.2 \times 10^{-31}$ cm^6/s, $C_{p\,LLI} = 9.9 \times 10^{-32}$ cm^6/s, $C_{HLI} = 1.66 \times 10^{-30}$ cm^6/s), and radiative recombination ($B = 9.5 \times 10^{-15}$ cm^3/s). The mobility of electrons and holes was fixed at 1360 and 470 cm^{2}V^{-1}s^{-1}, respectively. Bulk SRH recombination was made negligible by setting $\tau_{n0} = \tau_{p0} = 10^{12}$ μs and $E_t = E_i$. The surface recombination velocity was varied (where in PC1D, the electron and hole recombination velocities were equal, $S_n = S_p$). Boltzmann statistics and 100% ionisation were instituted.

To determine J_{0E} in PC1D, identical diffusion were introduced to the front and rear surfaces and the width was 500 μm. J_{0E} was determined for a range of excess carriers by setting the front illumination at 1190 nm and varying the intensity from 10,000 to 0.0001 W/cm^2 in logarithmic steps. This gave very close to uniform generation and therefore a symmetrical carrier profile. At each intensity, the J_{0E} was determined by taking the net recombination, subtracting the bulk Auger and radiative recombination, and dividing by $2 \cdot p \cdot n / (q \cdot n_i^2)$ where p and n were the carrier concentrations at 497 μm. By this method, J_{0E} was found to be constant over a wide range of Δn, increasing from about $\Delta n > 10^{15}$ cm^{-3}. Figure 1 shows the J_{0E} for $\Delta n < 10^{15}$ cm^{-3}. In EDNA 2, J_{0E} was determined at a junction voltage of 0.55 V.

A.2 Comparison of EDNA 2 to Sentaurus

The temperature was 300 K. The bulk was *p*-type with $N_A = 1 \times 10^{14}$ cm^{-3}. The diffusion was *n*-type with a Gaussian profile defined by a depth factor of 0.5 μm and a variable surface concentration. Identical models were applied for determining the intrinsic band gap (Sentaurus with a band gap multiplier of 1.00547), the density of states (Sentaurus Formula 1), band gap narrowing (Schenk), carrier mobility (Klaassen), Auger recombination (Altermatt), and radiative recombination ($B = 4.73 \times 10^{-15}$ cm^3/s). Bulk SRH recombination was included with $\tau_{n0} = \tau_{p0} = 100$ μs and $E_t = E_i$. The effective surface recombination velocity was varied. Fermi–Dirac statistics and 100% ionisation were instituted. J_{0E} was determined at a junction voltage of 0.65 V.

The device that was modelled in Sentaurus had a width in the *x*-dimension of 200 μm and contained four contacts. Two contacts were located on the front surface and two on the rear. On both front and rear, the contacts were 2 μm wide and located at the outer edges (leaving 196 μm between the contacts). The contacts were sufficiently small that contact recombination contributed negligibly to the total recombination in the diffusion, and the lateral variation in the J_{0E} was also negligible. The J_{0E} was calculated from $p \cdot n$ at 0.65 V, $p_0 \cdot n_0$ at 0 V, and the hole current density J_p, at a position very close to the metallurgical junction, using the equation $J_p = J_{0E} \cdot (p \cdot n / p_0 \cdot n_0)$.